

Assembly and Disassembly of Magnetic Mobile Micro-Robots towards Deterministic 2-D Reconfigurable Micro-Systems

Eric Diller*, Chytra Pawashe[†], Steven Floyd[‡] and Metin Sitti[§]

Abstract

A primary challenge in the field of reconfigurable robotics is scaling down the size of individual robotic modules. We present a novel set of permanent magnet modules that are under 1 mm in all dimensions, called Mag- μ Mods, for use in a reconfigurable micro-system. The modules are actuated by oscillating external magnetic fields of several mT in strength, and are capable of locomoting on a 2-D surface. Multiple modules are controlled by using an electrostatic anchoring surface, which can selectively prevent specific modules from being driven by the external field while allowing others to move freely. We address the challenges of both assembling and disassembling two modules. Assembly is performed by bringing two modules sufficiently close that their magnetic attraction causes them to combine. Disassembly is performed by electrostatically anchoring one module to the surface, and applying magnetic torques from external sources to separate the unanchored module.

1 Introduction

The field of reconfigurable robotics proposes versatile robots that can reform into various configurations depending on the task at hand (Yim et al. (2007)). These types of robotic systems consist of many independent and often identical modules, each capable of motion, and capable of combining with other modules to create assemblies. These modules can then be disassembled and reassembled into alternate configurations. For example, Shen et al. (2008) demonstrate SuperBot; this robot consists of 20 modules that can combine to form a mobile mechanism that can roll across the ground for 1 km and then reconfigure into one that can climb obstacles.

Another concept in the field of reconfigurable robotics is *programmable matter*, which is matter that can assemble and reconfigure into arbitrary three-dimensional (3-D) shapes, giving

rise to *synthetic reality* (Goldstein et al. (2005)). This is similar to virtual or augmented reality, where a computer can generate and modify an arbitrary object. However, in *synthetic reality*, this object has physical realization. A primary goal for *programmable matter* is scaling down the size of each individual module, with the aim of increasing spatial resolution of the final assembled product. Currently, the smallest deterministic, actuated module in a reconfigurable robotic system fits inside a 2 cm cube (Yoshida et al. (2001)), which is a self-contained module that is actuated using shape memory alloy. Scaling down further into the sub-millimeter scale brings new issues, including module fabrication, control, and communication.

Micro-robotics technologies of the past few years have been progressing (Sitti (2007, 2009)), with the introduction of externally actuated untethered mobile micro-robots under 1 mm in size; these robots can potentially be used as micron-scale modules. External actuation is necessary at this scale because it is currently not possible to fully integrate a power and actuation mechanism into a mobile device at the sub-millimeter scale. The micro-robots that operate on two-dimensional (2-D) surfaces in the literature can be controlled either electrostatically (Donald et al. (2006)), electromagnetically (Pawashe et al. (2009c); Vollmers et al. (2008)), or using laser thermal excitation (Sul et al. (2006)). 3-D swimming micro-robots are also possible, and are often electromagnetically controlled (Ergeneman et al. (2008); Martel et al. (2009)), and can even be powered by bacteria (Behkam and Sitti (2007); Martel et al. (2009)).

Methods for stochastic self assembly have been demonstrated at the micro- and nano-meter scale, as reviewed in Mas-trangeli et al. (2009). While the assembly conditions for these assemblies can be altered to create different shapes (Sawetzki et al. (2008)), the assembly process is itself stochastic, usually requiring random excitation and long periods of time for assembly. In addition, disassembly and reconfiguring of such assemblies is also stochastic in nature.

For the purposes of micron-scale assembly using micro-robots, Donald et al. (2008) demonstrate the assembly of four MEMS-fabricated silicon micro-robots, each under 300 μ m in all dimensions, actuated by electric fields. Once assembled however, they cannot detach and reconfigure, because the electrostatic driving fields do not allow for disassembly. Lipson et al. have demonstrated reconfigurable assemblies using 500 μ m planar silicon elements (Tolley et al. (2008)) and cm-scale 3-D elements (Kalontarov et al. (2010)). By controlling the local fluid flow in these systems, the elements can be deterministically assembled and disassembled into target shapes. This

*E. Diller and C. Pawashe are equally-contributing authors. E. Diller is with the Department of Mechanical Engineering, Carnegie Mellon University, Pittsburgh, PA 15213, USA

[†]C. Pawashe was with the Department of Mechanical Engineering, Carnegie Mellon University, Pittsburgh, PA 15213, USA and is currently with Intel Corporation, Portland OR 97124, USA

[‡]S. Floyd was with the Department of Mechanical Engineering, Carnegie Mellon University, Pittsburgh, PA 15213, USA and is currently with Arete Associates, Arlington VA 22202, USA

[§]M. Sitti is with the Department of Mechanical Engineering and Robotics Institute, Carnegie Mellon University, Pittsburgh, PA 15213, USA; correspondence can be made to: msitti@andrew.cmu.edu

system relies on an active substrate to provide fluid flow and control and so the assembled micron-scale elements have limited mobility. As a result, disassembling and reconfiguring fully deterministic mobile micron-scale modules is currently an unsolved problem.

We first introduced a reconfigurable set of magnetic micro-modules in Pawashe et al. (2009b), where the concept was described and initial experimental results were discussed. In this work, we present a more complete model of module assembly and disassembly processes with measurements of all relevant forces taken to compare with the models. A method to infer micro-scale properties of magnetic objects *in-situ* using magnetic fields is also proposed and used with the model. As a potential mobile reconfigurable system at the micrometer scale, the magnetic module system proposed in this paper is a step towards the creation of programmable reconfigurable assemblies.

The contribution of this work is to identify and analyze the conditions for micron-scale module assembly and disassembly. We identify the effects of important physical parameters in these processes through approximate analytical models and compare with empirical data. This information can be used for the design of more complex micro-scale reconfigurable systems using Mag- μ Mods or another platform.

The paper is organized as follows: Section 2 introduces the reconfigurable micro-robot system concept used and Section 3 describes the experimental setup used. Section 4 presents an analytical model of module assembly and disassembly and Section 5 presents the experimental results. The paper is concluded in Section 6.

2 Concept

In this work, we propose using sub-millimeter scale untethered permanent magnet micro-robots (Mag- μ Bots) actuated by external magnetic fields (Pawashe et al. (2009c)) as components of magnetic micro-modules (Mag- μ Mods), for creating deterministic reconfigurable 2-D micro-assemblies; this implies that the Mag- μ Mods will be able to both assemble and disassemble. Strong permanent magnet modules will attract each other with large magnetic forces; therefore it is necessary to reduce this magnet force between modules to facilitate disassembly. This can be done by adding an outer shell to the Mag- μ Bot for the design of a module. The outer shell prevents two magnetic modules from coming into close contact, where magnetic forces will become restrictively high. However, they are still sufficiently close together to yield a mechanically stable assembly. This shell-based Mag- μ Mod is shown in Figure 1. Alternatively, a Mag- μ Bot can be magnetized to a magnetization value less than its saturation value, and then be used as a Mag- μ Mod; this is a shell-less Mag- μ Mod.

Motion of multiple Mag- μ Mods is achieved by employing a surface divided into a grid of cells, where each cell on the surface contains an addressable electrostatic trap capable of anchoring individual Mag- μ Mods to the surface by capacitive coupling; this prevents them from being actuated by the external magnetic fields. This approach is related to that found in the field of *distributed manipulation* (Bohringer (1999)), where

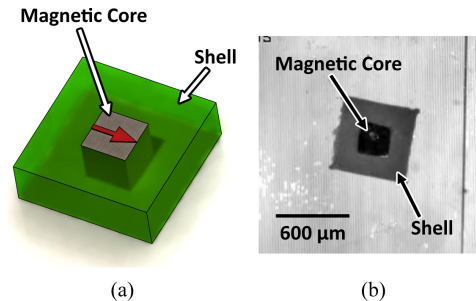


Figure 1: (a) Conceptual schematic of a shell-based Mag- μ Mod. A permanent magnet core is surrounded by a magnetically inactive shell. (b) Photograph of a Mag- μ Mod on an electrostatic anchoring surface. A magnetic core with approximate dimensions $300 \times 300 \times 170 \mu\text{m}^3$ is surrounded by a shell approximately $600 \times 600 \times 270 \mu\text{m}^3$ in outer dimensions.

parts are manipulated in parallel using programmable force fields, but here the distributed cells provide only a retarding force while the actuation magnetic force is globally applied to all modules. Unanchored Mag- μ Mods can move on the surface due to the imposed magnetic fields, and move in parallel. This technique is identical to controlling multiple Mag- μ Bots, explained in detail in Pawashe et al. (2009a). Assembling two Mag- μ Mods is straightforward – by moving an unanchored Mag- μ Mod towards an anchored one, magnetic forces eventually dominate and cause the two Mag- μ Mods to self-assemble.

For disassembly of two Mag- μ Mods to occur, the magnetic attraction between them must be overcome and the two separated. To do this, we use the electrostatic grid surface to anchor parts of assembled modules, and examine the effectiveness of externally applied magnetic torques to disassemble unanchored modules from the assembly.

Figure 2 shows the concept of multiple Mag- μ Mods assembling, disassembling, and reconfiguring into a different configuration. Because the Mag- μ Mods are magnetic, they can only assemble into configurations that are magnetically stable, implying that they form single closed flux loops.

Four Mag- μ Mods are operated in Figure 3 to demonstrate that they can create configurations, and reconfigure into other morphologies. From this experiment, the modules initially assemble into a magnetically stable ‘T’ configuration, and then reconfigure into a line configuration that is capable of translation.

3 Experimental Setup

Mag- μ Mods are actuated by six independent electromagnetic coils (shown in in Figure 4), aligned to the faces of a cube approximately 8.2 cm on a side. Depending on the required magnetic fields and gradients, the coils can contain either an air core or an iron core. Properties of the electromagnetic system are provided in Table 1. Maximum fields or gradients correspond to using two coaxial coils on opposite sides driven at maximum current, and are measured using Hall effect sensors (Allegro 1321) placed in the micro-robot workspace. Gradients

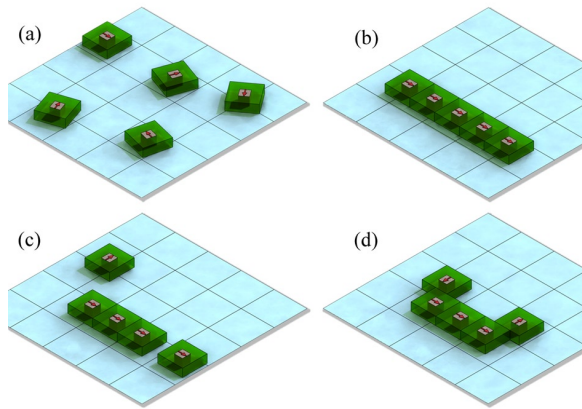


Figure 2: Schematic of five Mag- μ Mods operating on an electrostatic grid surface, where each cell can be individually activated to anchor-down individual Mag- μ Mods; unanchored Mag- μ Mods can be moved by the global magnetic field. (a) The five Mag- μ Mods are separate, and (b) assemble into a magnetically-stable line. In (c), the two outer Mag- μ Mods disassemble from the line, and (d) reconfigure into a magnetically stable ‘U’ shape.

are determined by measuring the field difference between two points spaced 1 mm apart. Control of the currents driving the electromagnetic coils are performed by a PC with a data acquisition system at a control bandwidth of 10 kHz, and the coils are powered by linear electronic amplifiers.

Actuation of each Mag- μ Mod is accomplished by using two or more electromagnetic coils. One or more horizontal coils are first enabled (coil D in Figure 4), causing the Mag- μ Mod to orient in the direction of the net magnetic field. Vertical clamping coils (coils C and F in Figure 4) are enabled and pulsed using a sawtooth waveform. This results in a non-uniform rocking motion of the Mag- μ Mod, which induces stick-slip motion across the surface. In general, the Mag- μ Bot’s velocity increases with pulsing frequency (typically from 1-200 Hz), and can exceed velocities of 50 mm/s in air. The Mag- μ Mod is also capable of operating in fluids of viscosities less than about 50 cSt, and can operate on a variety of smooth and rough magnetically inactive surfaces, provided that the adhesion between the Mag- μ Mod and surface is low. Further explanation of this locomotion method is given in (Floyd et al. (2009); Pawashe et al. (2009a,c)) and demonstration movies can be found online¹.

3.1 Mag- μ Bot and Mag- μ Mod Fabrication

Mag- μ Bots can be produced in a batch process using a molding technique, as described in Imbaby et al. (2008). The Mag- μ Bots used in this work are rectilinear and composed of a mixture of neodymium-iron-boron (NdFeB) particles (Magnequench MQP-15-7, refined in a ball mill to produce particles under 2 μ m in size) suspended in a polyurethane (TC-892, BJB enterprises) matrix in a ratio of 1 part polyurethane to 4 parts NdFeB by weight. This material is referred to as

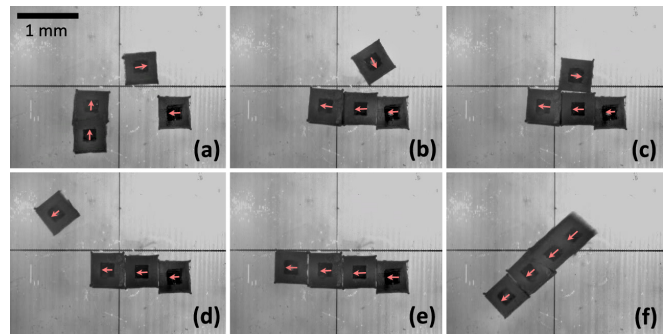


Figure 3: Frames from a movie with four teleoperated Mag- μ Mods (species MR2) assembling into a reconfigurable structure (video available in Extension 1). Arrows indicate direction of magnetization. (a) Four Mag- μ Mods prepare for assembly. (b) Three modules are assembled, and the fourth approaches. (c) All four modules are assembled. (d) One module is broken free using the rotation method from Section 4.5. (e) The module reattaches in a new configuration. (f) The new assembly is mobile, and is shown moving to a new location.

Property	Value	Units
Number of turns	140	–
Resistance	0.4	Ω
Wire diameter	1.15	mm
Coil length	3.2	cm
Inner diameter	5.1	cm
Distance to workspace	4.1	cm
Max driving current	19	A
Core length	10.1	cm
Max field at workspace (air core)	12.0	mT
Max gradient at workspace (air core)	0.44	T/m
Max field at workspace (Fe core)	49	mT
Max gradient at workspace (Fe core)	2.2	T/m

Table 1: Properties of the electromagnets.

Magnetic-Particle-Impregnated-Polyurethane (MPIP). The fabrication process is described in detail in Pawashe et al. (2009c).

A shell-less Mag- μ Mod is a Mag- μ Bot created with a lower value of magnetization. To do this, the standard fabrication steps are used, but the final magnetization step is performed in a smaller magnetic field. A shell-based Mag- μ Mod has a non-magnetic shell encasing a ferromagnetic core (the Mag- μ Bot). The shells are fabricated in a manner similar to the Mag- μ Bot, substituting aluminum powder for the magnetic powder to create aluminum-impregnated polyurethane (ALIP, in a ratio of 1 part polyurethane to 1 part aluminum powder by weight), which is used to make the shells partially conductive; this increases the electrostatic anchoring force by increasing the total area of conductive material.

The shell-less Mag- μ Mods are refined in a laser-milling system due to their rough edges from molding, while the ALIP

¹NanoRobotics Laboratory
<http://nanolab.me.cmu.edu/projects/MagneticMicroRobot/>

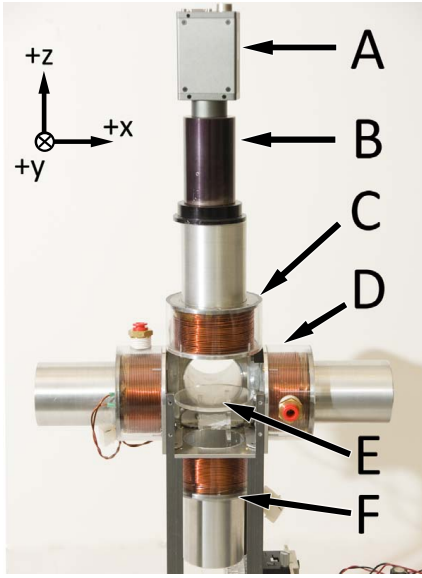


Figure 4: Photograph of the electromagnetic coil setup. A: camera for visual feedback, B: microscope lens, C: top $+z$ coil, D: one of four horizontal coils (the $+x$ coil in particular), E: experiment workspace, and F: bottom $-z$ coil. The $-y$ coil is removed to allow viewing of the workspace.

shells are used directly from the molding process.

Assembly of the ferromagnetic core into a shell is performed manually using tweezers under an optical microscope, and the two components are held together by UV curable epoxy (Loctite 3761). Figure 1(b) displays an assembled Mag- μ Mod. In the presence of the global magnetic fields, these modules move similarly to individual Mag- μ Bots without shells, exhibiting stick-slip motion across the working surface, however at lower velocities of about 0.5 mm/s.

Three shell-less and three shell-based species of Mag- μ Mods are used in this study, with properties listed in Table 2. Magnetic moments (m) were measured in a vibrating sample magnetometer (ADE Technologies Inc.), and dimensions were measured in an optical microscope with an error of $\pm 10 \mu\text{m}$. Module shell and core dimensions were chosen to cover a range of sizes which allow for the creation of stable assemblies which can be disassembled with the field strengths available, with an upper size limit of 1.0 mm. The buoyant weight (W_b) of each module are empirically determined by finding the minimum z -directed magnetic field gradient ($\frac{dB_{ec,z}}{dz}$ in Table 2) required to levitate it in silicone oil (as used in the experiments), and using (2), giving $W_b = m \frac{dB_{ec,z}}{dz}$. In this measurement, only the $+z$ coil is utilized, causing the Mag- μ Mod to orient and move in the $+z$ -direction. $\frac{dB_{ec,z}}{dz}$ has an estimated error of 25 mT/m and W_b has up to $\pm 14\%$ error.

3.2 Electrostatic Grid Surface Fabrication

The electrostatic grid surface, described in Pawashe et al. (2009a), is used to enable the control of multiple Mag- μ Bots or Mag- μ Mods. It consists of an array of independently addressable pads, each pad containing a set of interdigitated electrodes

to generate high electric fields. Mag- μ Mods are placed on this surface and are operated in a low-viscosity silicone oil (Dow Corning 200 fluid, 20 cSt, with density of $\rho_{oil} \approx 950 \text{ kg/m}^3$) which supports the generation of the large electric fields required to anchor individual Mag- μ Mods. Anchoring occurs through a capacitive coupling force to the surface for conductive materials.

4 Modeling

In modeling the operation of a Mag- μ Mod, we are interested in its interactions with the externally applied magnetic fields, electrostatic fields from the surface, magnetic fields from other Mag- μ Mods, and surface effects such as adhesion and friction at the micro-scale. Figure 5 displays a typical static configuration of two assembled Mag- μ Mods, M1 and M2. Nomenclature for the forces and torques acting on modules are given in Table 3.

Term	Definition
m	Module magnetic moment
M	Module magnetization per volume
V	Module magnetic core volume
\vec{B}_i	Module magnetic field
\vec{B}_{ec}	Externally applied magnetic field
\vec{F}_{ec}	Externally applied magnetic force
\vec{T}_{ec}	Externally applied magnetic torque
\vec{F}_i	Magnetic force between modules
\vec{T}_i	Magnetic torque between modules
$F_{s,f}$	Module to surface adhesive force for area contact
$F_{s,e}$	Module to surface adhesive force for line contact
$F_{s,i}$	Adhesive force between modules
F_e	Electrostatic anchoring force to the surface
N	Reaction normal force from the surface
N_i	Reaction normal force between modules
F_f	Friction force from the surface
$F_{f,i}$	Friction force between modules
W_b	Buoyant weight

Table 3: Select nomenclature.

4.1 Magnetic Influences

Each magnetized Mag- μ Mod creates a magnetic field of $\vec{B}_i(x, y, z)$, and the six external electromagnets create a magnetic field of $\vec{B}_{ec}(x, y, z)$. Magnetic torques exerted on Mag- μ Mods are proportional to the magnetic field strength, and act to bring their internal magnetizations into alignment with the field. The magnetic forces exerted on Mag- μ Mods are proportional to the spatial gradient of the magnetic field, and act to move them to a local maximum. The magnetic torques and

Species	Core Size (μm^3) L×W×H	Shell Size (μm^3) L×W×H	m (mEMU)	$\frac{dB_{ec,z}}{dz}$ (mT/m)	W_b (μN)
MR1	225 × 250 × 180	848 × 837 × 271	0.83	1340	1.10 ± 0.02
MR2	215 × 225 × 172	541 × 565 × 249	1.0	946	0.95 ± 0.03
MR3	110 × 115 × 97	318 × 328 × 232	0.20	1200	0.23 ± 0.01
MR4	500 × 530 × 170	–	2.6	187	0.48 ± 0.06
MR5	413 × 421 × 177	–	2.0	213	0.42 ± 0.05
MR6	298 × 298 × 200	–	0.87	224	0.19 ± 0.01

Table 2: Measured properties of the Mag- μ Mods. Measurements of $\frac{dB_{ec,z}}{dz}$ are used to calculate the buoyant weight **W_b**. Modules are magnetized along the length dimension.

forces are determined using the general relations, integrating over volume of the magnet (Cheng (1992)):

$$\vec{T}_m = \int_V \vec{M} \times \vec{B}(x, y, z) dV \quad (1)$$

$$\vec{F}_m = \int_V (\vec{m} \bullet \vec{\nabla}) \vec{B}(x, y, z) dV \quad (2)$$

where \vec{T}_m and \vec{F}_m are the general magnetic torques and forces the Mag- μ Mod experiences, respectively, and \vec{M} is the magnetization vector of the Mag- μ Mod. $\vec{B}(x, y, z)$ is the total magnetic field at (x, y, z) , which is the summation of $\vec{B}_{ec}(x, y, z)$ and all $\vec{B}_i(x, y, z)$ from other Mag- μ Mods in the workspace. Far from the field source \vec{B} becomes relatively constant over the volume and these equations can be simplified to the single dipole approximation.

To approximate the forces and torques Mag- μ Mods exert on each other, the structure of the magnetic field generated by each Mag- μ Mod is required. To estimate these fields, Mag- μ Mods are modeled as distributed magnetic dipoles, with the total contribution to the field determined numerically. The field generated by these distributed magnetic dipoles is (Cheng (1992)):

$$\vec{B}(\vec{M}, \vec{r}) = \frac{\mu_0}{4\pi} \int_V \frac{1}{|\vec{r}|^5} [3\vec{r}(\vec{M} \cdot \vec{r}) - \vec{M}(\vec{r} \cdot \vec{r})] dV \quad (3)$$

where $\mu_0 = 4\pi \times 10^{-7}$ [H/m] is the permeability of free space and \vec{r} is the vector from the dipole to the point of interest. In practice, the magnetic volume is discretized into a finite number of magnetic dipoles for ease of calculation.

4.2 Surface Adhesion

Forces between the surface and a Mag- μ Mod can include capillary, electrostatic, and van der Waals effects (Israelachvili (1992)), and are here lumped together into one force, the magnitude of which can depend on whether the Mag- μ Mod is contacting the surface on an edge ($F_{s,e}$) or is lying flat ($F_{s,f}$). This force depends on the material properties of the Mag- μ Mod, surface, and environment.

For edge-contact, $F_{s,e}$ is estimated using a method depicted in Figure 6, where an applied magnetic field gradient in the z -direction ($\frac{\partial B_{ec,z}}{\partial z}$) is increased until the Mag- μ Mod lifts away

from the surface. The magnetic force ($F_{ec,z}$) due to this gradient must overcome W_b and $F_{s,e}$. A uniform x -directed field is also generated to orient the Mag- μ Mod at an angle θ with the surface, ensuring edge contact. $F_{s,e}$ can be calculated as:

$$F_{s,e} = F_{ec,z} - W_b = [m_1 \sin(\theta)] \frac{\partial B_{ec,z}}{\partial z} - W_b \quad (4)$$

$$\theta = \tan^{-1} \left(\frac{B_z}{B_x} \right) \quad (5)$$

Equation (5) assumes that \vec{m}_1 is parallel to \vec{B}_{ec} , which is appropriate since the imposed magnetic torques that support this relation dominate other torques. Additionally, N vanishes right before the Mag- μ Mod leaves the surface, and is not present in the relations.

For flat-contact adhesion, $F_{s,f}$ is estimated using a method depicted in Figure 7, where a known uniform $B_{ec,z}$ is applied to rotate the Mag- μ Mod away from the surface, causing it to pivot about P_r . The applied magnetic torque must overcome the torque exerted onto the Mag- μ Mod by $F_{s,f}$ and W_b , which are taken to act at the centroid of the Mag- μ Mod.

Considering the static condition of the Mag- μ Mod right before it rotates away from the surface, $F_{s,f}$ can be calculated as:

$$F_{s,f} = \frac{2m_1 B_{ec,z}}{L_m} - W_b \quad (6)$$

which assumes that \vec{m}_1 is orthogonal to \vec{B}_{ec} .

4.3 Sliding Friction

The friction coefficient (μ) between surfaces at the micro-scale can vary from bulk macro-scale values. Thus it is necessary to infer μ using micro-scale objects to obtain an accurate *in-situ* value. To estimate μ between a Mag- μ Mod and a surface, we apply known forces onto the Mag- μ Mod that cause it to slide on its edge with the surface, as shown in Figure 8. A magnetic field in the x and z -directions is applied to ensure the Mag- μ Mod is on its edge. The x -directed magnetic field gradient, $\frac{\partial B_{ec,x}}{\partial x}$, is then increased until the Mag- μ Mod slips, indicating that the static friction force has been overcome. Using a basic Coulomb friction relation, μ is estimated:

$$F_f = \mu N = \mu(W_b + F_{s,e} - F_{ec,z}) \quad (7)$$

$$\mu = \frac{F_{ec,x}}{W_b + F_{s,e} - F_{ec,z}} \quad (8)$$

$$F_{ec,x} = [m_1 \cos(\theta)] \frac{\partial B_x}{\partial x} \quad (9)$$

where \vec{m}_1 is assumed to be parallel to \vec{B} .

4.4 Assembly of Magnetic Micro-Modules

As two Mag- μ Mods with aligned magnetizations approach each other, their magnetic attraction increases due to the approximate r^{-3} dependence of their fields, from (3). At a critical separation distance, $d_{x,c}$, the attractive forces overcome other forces, causing the modules to self-assemble. This assembly process is illustrated in Figure 9.

To determine $d_{x,c}$, we assume that \vec{T}_m dominates other torques, and take M1's moment vector to align with \vec{B} . This implies:

$$\theta = -\tan^{-1}\left(\frac{B_z}{B_x}\right) \quad (10)$$

$$\vec{m}_2 = m_2 [\cos(\theta)\vec{a}_x - \sin(\theta)\vec{a}_z] \quad (11)$$

where \vec{a}_x and \vec{a}_z are unit vectors in the x and z -directions, respectively.

When M2 is about to assemble with M1, summing the forces in the x and z -directions from Figure 9 gives:

$$N = F_{s,e} + W_b - F_{ec,z} - F_{i,z} \quad (12)$$

$$F_{i,x} = F_f - F_{ec,x} \quad (13)$$

\vec{F}_i can be determined using \vec{B}_i with (2), and using \vec{m} from (11). \vec{B}_i from M1 can be determined using (3) with $\vec{m} = \vec{m}_1 = m_1\vec{a}_x$. \vec{F}_{ec} can be determined using (2) with the known applied \vec{B}_{ec} , and \vec{m}_2 from (11). \vec{r} in these computations

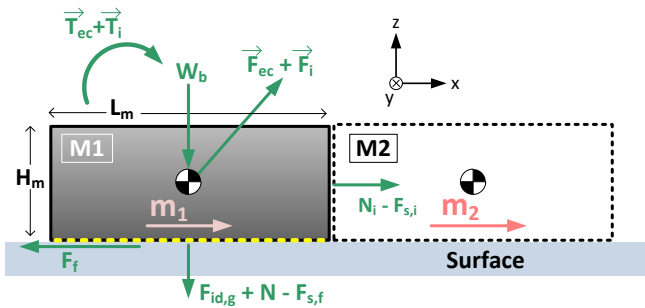


Figure 5: Side view schematic of two Mag- μ Mods assembled together. M1 is anchored to the surface, and forces and torques acting upon it are displayed. Relevant geometry and coordinates used in equations are shown.

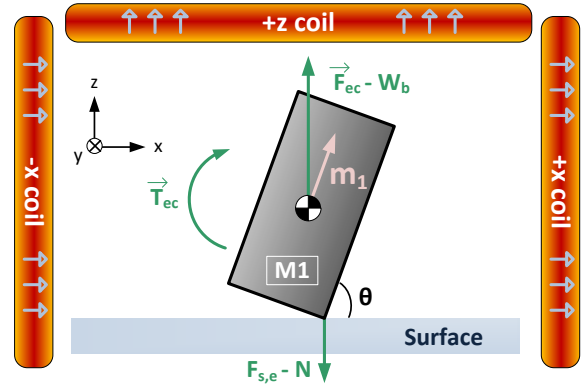


Figure 6: Free body diagram for estimating the edge-contact surface force, $F_{s,e}$. The $+z$, $-x$, and $+x$ coils create a magnetic field that orients the Mag- μ Mod at θ with the surface. A gradient in the $+z$ -direction is increased until the Mag- μ Mod lifts off the surface. No gradient in the x -direction is generated, and thus there is no x -directed force. Arrows on coils indicate direction of magnetic field generated by the coil.

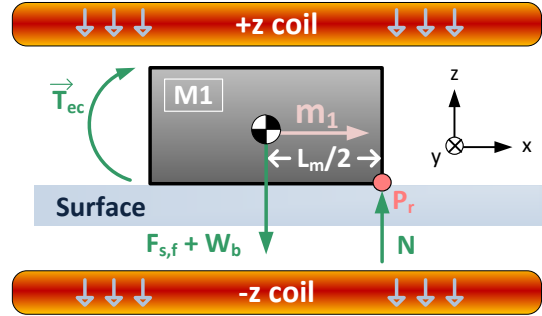


Figure 7: Free body diagram for estimating the flat-contact surface force. A uniform field is generated using the $+z$ and $-z$ coils. This field is increased until the Mag- μ Mod rotates about P_r , its pivot point with the surface. Arrows on coils indicate direction of magnetic field generated by the coil.

is calculated using the geometries in Figure 9 as:

$$\phi = \tan^{-1}\left(\frac{H_m}{L_m}\right) \quad (14)$$

$$d_z = \frac{1}{2}\sqrt{H_m^2 + L_m^2} \sin(\theta + \phi) - \frac{H_m}{2} \quad (15)$$

$$\vec{r} = -d_{x,c}\vec{a}_x + d_z\vec{a}_z \quad (16)$$

where d_z is the center-to-center distance from M1 to M2 in the z -direction.

Subsequently, $d_{x,c}$ can be numerically solved using (10)-(16). Surface forces and friction coefficients are determined using the methods in Section 4.2.

A layered assembly of two modules can be achieved by tilting the approaching module M2 up on its back edge so that it mounts the top of the anchored module as shown in Fig. 11(a).

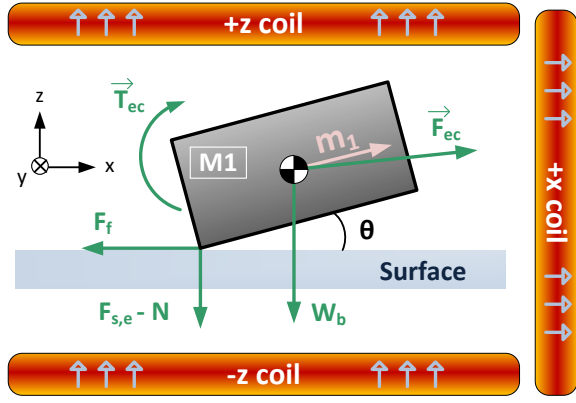


Figure 8: Free body diagram depicting the method for estimating the friction coefficient. The $+z$ and $-z$ coils create a uniform $+z$ -directed field. The $+x$ coil creates a $+x$ -directed field and gradient. The x -directed coil may use an iron core to increase the x -directed magnetic field gradient, which causes the Mag- μ Mod to slide on the surface.

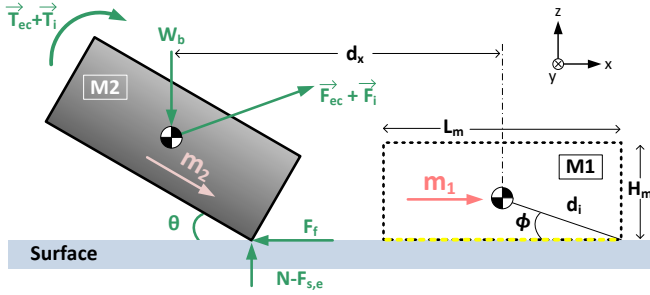


Figure 9: Schematic of two Mag- μ Mods, M1 and M2, assembling. M1 is anchored to the surface, and when M2 approaches the critical distance, $d_x = d_{x,c}$, the magnetic attractive force will pull M2 into contact with M1.

4.5 Disassembly of Planar Magnetic Micro-Modules

One set of methods to disassemble two modules that are assembled in the planar configuration from Figure 5 takes advantage of magnetic torques, which are generally stronger than magnetic forces at the micro-scale (Abbott et al. (2009)). One such rotational disassembly method is shown in Figure 10. The procedure for this disassembly method is:

1. The assembly of M1 and M2 is translated into a position where the electrostatic anchoring surface completely anchors M1 but leaves M2 free.
2. Using z -directed magnetic fields, M2 is rotated until it aligns with the z -axis, indicated by position M2'.
3. M2 is then further rotated until its magnetization opposes M1's, inducing a repulsive force; this position is M2''.
4. M2 simply walks away from M1 using a stick-slip translation procedure, which is now possible due to the repulsion between the two modules.

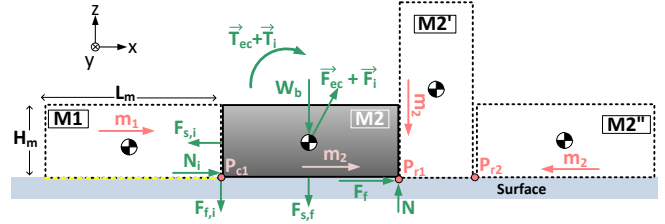


Figure 10: Schematic of two initially assembled modules, M1 and M2, throughout the rotational disassembly process. Module M1 is electrostatically anchored to the surface, while M2 is in the process of being disassembled to position M2', and then to M2''.

The required external magnetic fields to rotationally disassemble M2 from M1 can be determined by analyzing the forces M2 experiences. We are primarily interested in the most difficult disassembly step, which is when M2 is initially assembled with M1 and moves to M2'. The static case is taken where M2 begins to rotate about the contact point P_{r1} ; this implies that N acts at P_{r1} , and the normal force between M2 and M1, N_i , acts at P_{c1} . To determine the required \vec{B}_{ec} to perform this step, we sum the in-plane torques on M2 about P_{r1} and use (1), giving:

$$T_{ec,y} = -T_{i,y} - (F_{i,x} + F_{ec,x} - F_{s,i}) \frac{H_m}{2} \quad (17)$$

$$- (F_{i,z} + F_{ec,z} - W_b - F_{s,f} - 2F_{f,i}) \frac{L_m}{2}$$

$$B_{ec,z} = \frac{T_{ec,y}}{m_2} \quad (18)$$

Since uniform z -directed magnetic fields are used in this procedure, $\vec{F}_{ec} = 0$.

\vec{F}_i can be determined using (2) with (3), where $\vec{r} = L_m \vec{a}_x$, $\vec{m} = m_1 \vec{a}_x$ for determining \vec{B}_i , and $\vec{m} = m_2 \vec{a}_x$ for determining \vec{F}_i . Similarly, \vec{T}_i can be determined using (1) with (3). $F_{s,i}$ and $F_{s,f}$ are determined with the methods in Section 4.2. $F_{f,i}$ is the friction force between M2 and M1 before M2 slips on M1. $F_{f,i}$ and N_i can be determined using Figure 10 by summing the forces in the x -direction, and taking $F_f = 0$ since M2 is supported by M1 in the x -direction:

$$N_i = F_{s,i} + F_{i,x} \quad (19)$$

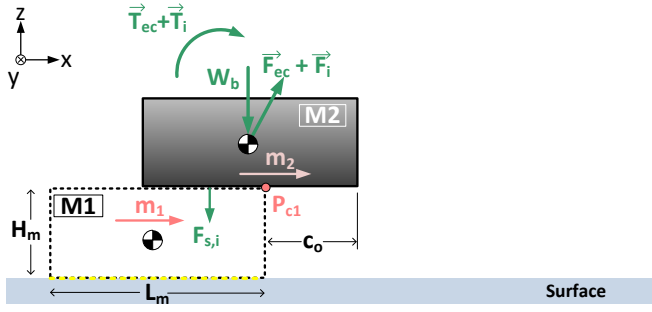
$$F_{f,i} = \mu_i N_i \quad (20)$$

Thus with (17)-(20), the minimum \vec{B}_{ec} can be found that accomplishes the Mag- μ Mod rotation described in Figure 10.

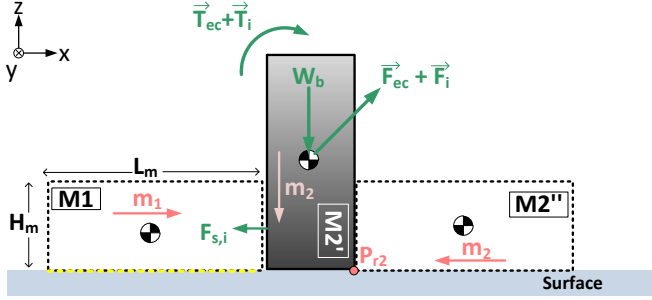
4.6 Disassembly of Layered Magnetic Micro-Modules

Mag- μ Mods can assemble to form a layered configuration that retains a significant total magnetization, as shown in Figure 11(a). From Figure 11(b), the procedure for disassembly is:

1. The combined modules M1 and M2 are translated into a position where the electrostatic anchoring surface completely anchors M1. M2 is far enough from the surface



(a) Two Mag- μ Mods, M1 and M2, are initially assembled in a layered configuration.



(b) M2 disassembles from M1 using a rotational disassembly process. M1 is electrostatically anchored to the surface. M2 moves into position M2' about P_{c1} , and then into M2'' about P_{r2} , at which point it can walk away.

Figure 11: Schematic of two Mag- μ Mods disassembling from a layered configuration.

that it will not be affected by the electric fields from the electrostatic anchoring surface.

2. M2 is rotated about P_{c1} in Figure 11(a) until it aligns with the z -axis by using z -directed magnetic fields. The resulting configuration is shown as M2' in Figure 11(b).
3. M2 is then further rotated using $-x$ -directed magnetic fields until its magnetization points in the $-x$ -direction. The resulting configuration is shown as M2'' in Figure 11(b).
4. M1 and M2 are in a repulsive configuration with each other, and M2 can simply walk away from M1 using a stick-slip translation procedure.

The required external magnetic fields to rotationally disassemble M2 from M1 can be determined by analyzing the forces M2 experiences. From experimental observation, the most difficult step in this disassembly procedure is rotating M2 into M2' from Figure 11(b), and thus will be the focus of analysis. In Figure 11(a), M2 is initially assembled with M1; the static case is then taken where M2 just begins to rotate about the contact point P_{c1} . Because P_{c1} will not necessarily be located directly below the center of mass of M2, the weight of M2 will induce an additional torque about P_{c1} . To determine the required $B_{ec,z}$ to perform this step, the in-plane torques on M2 are summed about P_{c1} , and (1) is used, giving:

$$T_{ec,y} = -T_{i,y} - (F_{i,x} + F_{ec,x}) \frac{H_m}{2} \quad (21)$$

$$B_{ec,z} = \frac{T_{ec,y}}{m_2} \quad (22)$$

where c_o is the overhang of M2 from M1.

\vec{F}_i can be determined using (2) with (3), where $\vec{r} = (\frac{1}{2}L_m + c_o)\vec{a}_x + H_m\vec{a}_z$, and $\theta = 0$. Similarly, \vec{T}_i can be determined using (1) with (3). $F_{s,i}$ is determined experimentally using the methods in Section 4.2. In reality, these adhesion forces represents a pressure across the surface of M2; in analysis, it is taken to be a single force acting upon the centroid of the contact area between M1 and M2. The overhang distance, c_o , can be estimated by finding the c_o that minimizes the magnetostatic energy between the two modules. This can be performed by a numerical iterative process by finding the c_o that minimizes $F_{i,x}$ on M2 using (2) and (3).

Thus with (21)-(22), \vec{B}_{ec} can be solved to accomplish the Mag- μ Mod disassembly described in Figure 11.

5 Experimental Results and Discussion

In the surface force and friction experiments, Mag- μ Mods are operated on a glass or polyurethane (PU) surface; the glass surface simulates a glass-based electrostatic anchoring surface, while the PU surface replicates a module's surface. Electromagnetic fields and gradients are measured post-experiment by placing a Hall sensor at the location of the Mag- μ Mod and recreating the currents through the coils used in the experiments.

In the assembly and disassembly experiments, a simplified environment is used where one Mag- μ Mod is glued onto a glass surface to simulate electrostatic anchoring. In the demonstration experiments, a glass-based electrostatic anchoring surface with four anchoring pads in a 2×2 configuration is utilized. Motion is achieved by pulsing the electromagnetic coils from 1-10 Hz using a sawtooth waveform. All experiments are performed in a silicone oil fluid environment.

In all experiments, at least three trials are performed to determine repeatability and error. In all data sets, errors are considered from all known sources. All measurements reported were taken in a single day. Module surface properties such as friction and adhesion have been observed to change over the course of several weeks, but over a single day the properties are very consistent. This was verified by repeating experiments over the course of day and demonstrating a low degree of variability as shown in the data presented here. The longer-term changes in properties (observed to change by a relative error up to 200%) are possibly due to differences in temperature and humidity, absorption of liquid into the module bodies over time as well as oxidation of the magnetic material resulting in a decreased magnetic moment. These effects can possibly be stabilized by storing the modules in their operation environments or by using more stable materials.

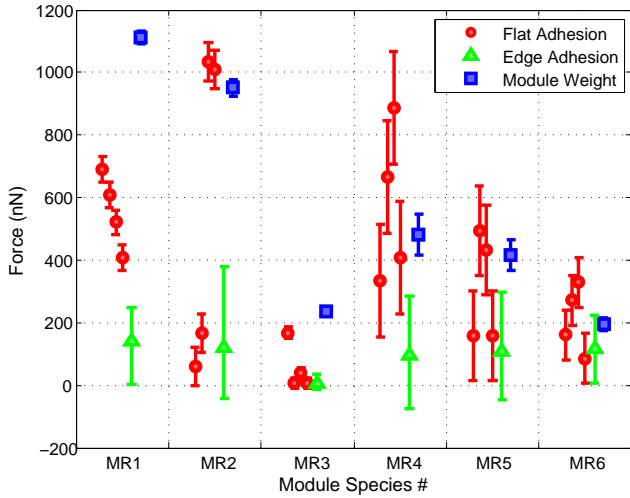


Figure 12: The adhesive force between the Mag- μ Mods and a glass surface for the flat case ($F_{s,f}$) and the edge case ($F_{s,e}$). The four flat adhesion plots correspond to experiments performed on each of the four edges of each module. Module weight is also shown for comparison.

To use (3) in computation, each permanent magnetic body was taken as at least 4^3 dipoles, evenly distributed throughout the magnetic body. This was found to be less than 3% different from a solution with 5^3 dipoles. A larger number of dipoles will lead to a more accurate solution, but with higher computational expense.

5.1 Surface Adhesion

Using the experiment and models described in Section 4.2, the surface forces are determined between the Mag- μ Mod and a surface. Figure 12 shows the forces for a glass surface, and Figure 13 shows the forces for a polyurethane surface. The weight of each Mag- μ Mod is displayed for comparison. Data used to compute these forces are available in Extension 3.

In general, $F_{s,e}$, determined with the method from Figure 6, is similar among all the Mag- μ Mod species, indicating that the difference in size among the modules does not affect the edge-based adhesion. Since adhesion is normally area dependent, it would be expected that a Mag- μ Mod with a larger edge would experience larger adhesive forces. However, it is likely that the modules are contacting the surface with their asperities due to large surface roughnesses, implying that the effective area of contact is similar for all species.

$F_{s,f}$, determined with the method from Figure 7, can vary among Mag- μ Mods and is seen to have large experimental error. In this experiment, modules were rotated from each of the four possible edges, as during assembly or disassembly. This is shown in the figures by the four flat adhesion values plotted for each module species. Due to the nature of the experiment, the assumption that the adhesive force is acting upon the module's COM may be incorrect. At one extreme, the asperities will be at opposite ends (separated by a distance L), and at the other extreme we assume a rounded bottom face such that the

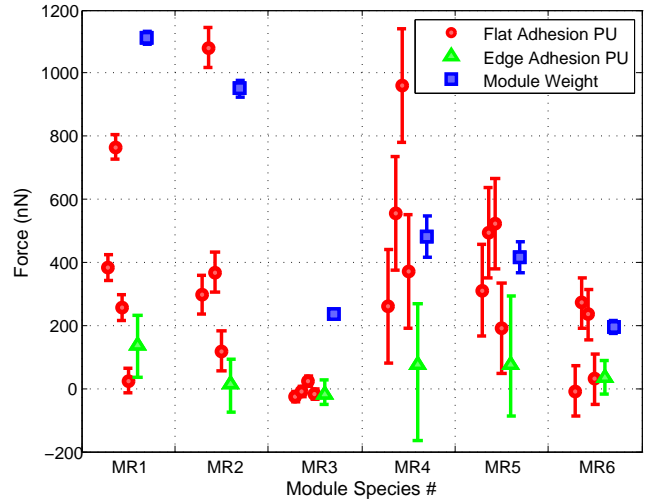


Figure 13: The adhesive force between the Mag- μ Mods and a polyurethane surface for the flat case ($F_{s,f}$) and the edge case ($F_{s,e}$). The four flat adhesion plots correspond to experiments performed on each of the four edges of each module. Module weight is also shown for comparison.

Mag- μ Mod would rotate so that the effective asperity separation would be zero. Therefore, ignoring other sources of error, the experiment could give values of flat adhesion from zero to double the actual $L/2$ average value. This wide spread of adhesion values is seen between the edges, especially for species MR2. When these data are used later as surface parameters in the analytical model, the average value and standard deviation from all four edges is used because it is difficult to determine which edge the module is rotating about. Comparing measured adhesion values between a glass surface and polyurethane surface, there is not significant difference.

Some measurements result in slightly negative adhesion, or repulsion from the surface. The methods described in Section 4.2 should not be able to give a negative value as any repulsion from the surface will not assist the Mag- μ Mod in rotating away from the surface in the flat-adhesion measurement method, or lift away from the surface in the edge-adhesion measurement method. Therefore, the few negative adhesion values obtained are considered erroneous.

5.2 Sliding Friction

Using the experiment and models described in Section 4.3, the friction coefficient is determined between the Mag- μ Mod and a surface. Figure 14 shows the friction coefficient for a glass surface and polyurethane surface. Data used to compute these forces are available in Extension 3.

For the friction coefficients on a glass surface, there is not a significant difference among the Mag- μ Mods; the shell-less modules experience on average a slightly higher friction coefficient. On a polyurethane surface, it is clear that the shell-less Mag- μ Mods, which contact the surface with MPIP, are exhibiting higher friction coefficients than the shell-based Mag- μ Mods, which contact the surface with its ALIP shell. This

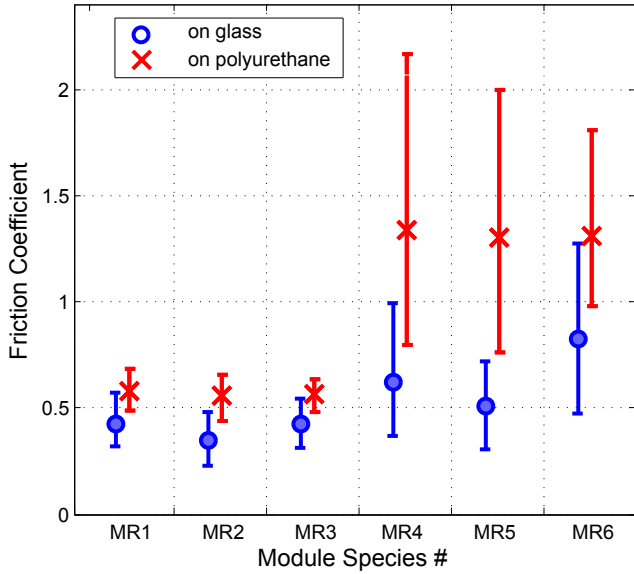


Figure 14: The friction coefficient between the Mag- μ Mod and a surface of glass and polyurethane.

difference would indicate that the polyurethane that binds the metallic powders in ALIP and MPIP is not the exposed material. In fabrication, the shell-less Mag- μ Mods are refined in a laser-milling system, which can potentially expose the embedded NdFeB particles. The ALIP shells are not laser-refined and are taken directly from the molding process. This difference can lead to different sets of materials being in contact with the working surface, leading to different frictional properties.

5.3 Planar Assembly of Magnetic Micro-Modules

Mag- μ Mod assembly is performed using the method described in Section 4.4, and a demonstration of assembly is shown in Figure 15. To compare with the model in Section 4.4, each species of Mag- μ Mod is walked slowly towards a fixed Mag- μ Mod of the same species and is assembled. The jump-into distance is estimated from experimental video. A sawtooth waveform is used for walking actuation, with a maximum x and z -directed field of 1.3 mT. The x -directed magnetic field gradient is zero, since the $+x$ and $-x$ coils are used in equal opposition. The z -directed magnetic field gradient is 58 mT/m if the $+z$ -coil is used for pulsing, or -58 mT/m if the $-z$ -coil is used for pulsing. In model computations, $F_{s,e}$ is taken as the edge-adhesion data from Figure 12, and μ is taken from data in Figure 14.

Using the assembly model described in Section 4.4, along with surface forces and friction coefficients from Figures 12–14, the estimated $d_{x,c}$ is determined, and presented in Figure 16 for the case with a positive z -directed gradient, and in Figure 17 for the case with a negative z -directed gradient. Because it is unclear what angle θ the Mag- μ Mod is in experiment right before assembly occurs, two bounding cases are simulated: (1) $\theta = 0$ takes the case that the z -directed magnetic fields and gradients are zero, and (2) $\theta = \theta_{max}$ takes the case that the z -directed magnetic fields and gradients are at their maximum

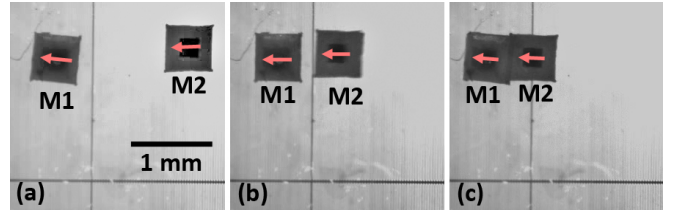


Figure 15: Frames from a movie showing two Mag- μ Mods (species MR2), M1 (anchored) and M2 (unanchored), assembling into a planar configuration (video available in Extension 2). (a)-(b) M2 walks towards M1, and both modules have aligned magnetizations. (c) The two modules assemble due to magnetic attraction forces. Direction of magnetization is shown on each module.

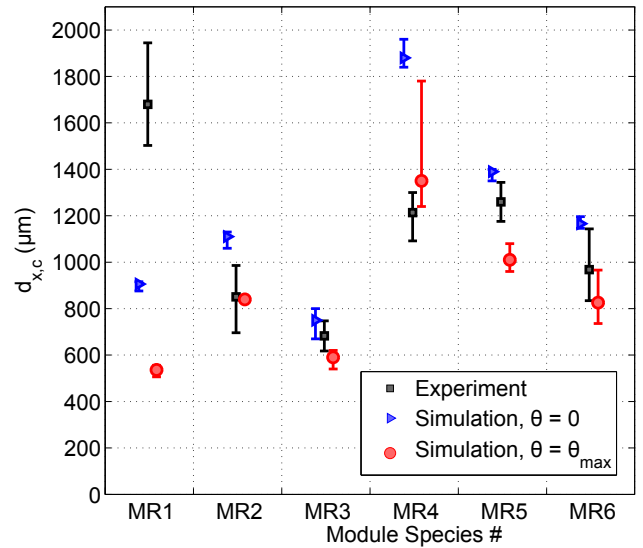


Figure 16: Experiment and simulation of the Mag- μ Mods assembling (with jump-into distance $d_{x,c}$), with a magnetic field gradient in the $+z$ -direction. In each experiment, one Mag- μ Mod is fixed on the surface, and the other walks towards it. Simulated data have error bars as empirically determined surface forces and friction are used in computation.

magnitude. From these results, the experimental $d_{x,c}$ in Figure 16 is bounded by the two simulated bounds and error ranges for all Mag- μ Mod species except for MR1.

Generally, $d_{x,c}$ is slightly larger for the case of a positive z -directed gradient in the experiments. In this condition, a magnetic force acts to lift the Mag- μ Mod away from the surface, which in effect reduces N with the surface, and thus reduces F_f . A smaller friction force will provide less resistance to the magnetic attraction between two modules, and thus will jump-into contact at a longer range. In the simulations, $d_{x,c}$ is only slightly larger for the case of the positive z -directed gradient waveform in the $\theta = \theta_{max}$ case (the $\theta = 0$ case is identical in both simulation sets). The dependence of $d_{x,c}$ on θ can be significant, and the θ that occurs during jump-into contact can be different depending on whether a positive or negative z -directed gradient was used.

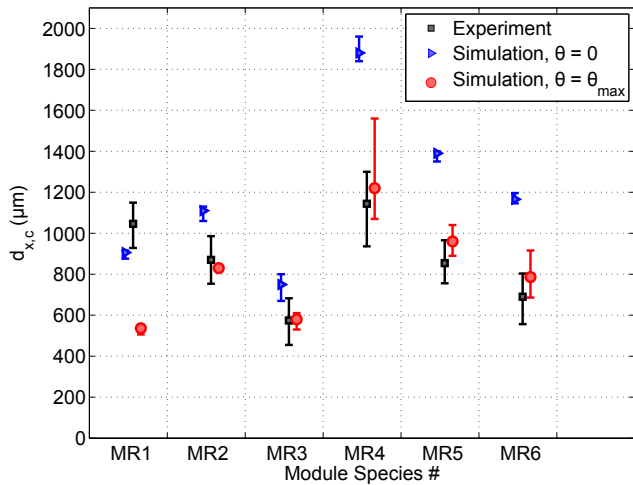


Figure 17: Experiment and simulation of the Mag- μ Mods assembling (with jump-into distance $d_{x,c}$), with a magnetic field gradient in the $-z$ -direction. In each experiment, one Mag- μ Mod is fixed on the surface, and the other walks towards it. Simulated data have error bars as empirically determined surface forces and friction are used in computation.

Another issue that is not considered in simulation is how F_f depends on the Mag- μ Mod's state. In the measurements, F_f comes from a static friction assumption; however, because the module translates using a stick-slip behavior, its point of contact with the surface can be sliding when jump-into contact occurs, and result in a smaller friction force, as kinetic friction is generally smaller than static friction. This effect could explain the disparity in the experiment and simulation for the case of MR1 in Figure 16.

5.4 Disassembly of Planar Magnetic Micro-Modules

For Mag- μ Mods that are assembled in a planar fashion (as in Figure 5), disassembly is performed using the method described in Section 4.5. A demonstration of this disassembly is shown in Figure 18. In the experiments, each species of Mag- μ Mod disassembles from another of the same species from an initially assembled state. The magnetic fields that begin to disassemble the Mag- μ Mods are recorded, and are compared to the estimates from the models in Section 4.5. These comparisons are shown in Figure 19, which also includes a simulation that considers $\mu_i = 0$, since it is unclear in the experiments whether the modules are in intimate contact. In model computations, $F_{s,f}$ is taken as the flat-adhesion data from Figure 12, $F_{s,i}$ is taken as the flat-adhesion data from Figure 13, and μ_i is taken from data in Figure 14.

From these results, it is not clear whether the friction between modules is important or not, and can be dependent on specific micro-modules. For MR3-MR5, the experimental results lie in the bounding cases within error, however the simulations underestimate the required $B_{ec,z}$ for MR1 and MR2, and overestimate the required $B_{ec,z}$ for MR6. Large simulation deviations are seen for MR4-MR6, which result from the large

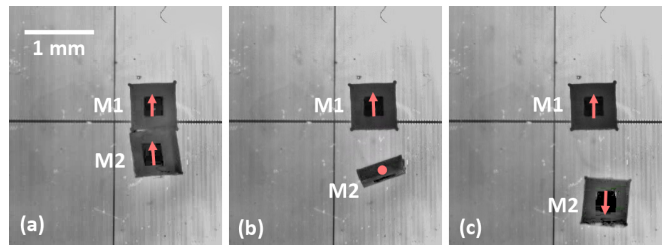


Figure 18: Frames from a movie showing two Mag- μ Mods (species MR2), M1 (anchored) and M2 (unanchored), disassembling from a planar configuration (video available in Extension 2). (a) Initial configuration. (b) M2 rotates into a vertical orientation with magnetization out of the page, and rotates further in (c) until it is in a repulsive orientation with M1. Direction of magnetization is shown on each module.

errors in the measurement in friction, shown in Figure 14.

One possible explanation for an underestimation in the required $B_{ec,z}$ is that the contact between two modules has interlocking asperities. This would cause a significantly higher required torque in order to rotate the disassembling module, as mechanical interlocking will be significantly stronger than the sliding friction model from the simulation. The shell-based modules (MR1-MR3) exhibit this behavior, which can have rough surfaces on their outside faces. The shell-less modules (MR4-MR6), which are refined in a laser after fabrication, may have smoother faces, reducing the chance of interlocking between modules. For MR4-MR6, the simulation bounds or overestimates the required $B_{ec,z}$, which may support a sliding friction assumption between the faces (although of uncertain N_i , thus an uncertain $F_{f,i}$).

It is unclear as to why MR6 is overestimated in both bounds from the simulation, which implies that there is more than just the inter-surface contact that can add error in these results. Other sources of error can include the possibility that the modules may not be perfectly aligned, and that a module's magnetization is not perfectly parallel with its length. Also because of the fabrication process, the density of the modules may not be uniform, and thus not have uniform magnetization. In particular, it is believed that there are air bubbles embedded inside the modules, which may not be uniformly distributed. As a result, the effective magnetic 'centers' of a Mag- μ Mod may not be its geometric center, and lead to skewed results for disassembly.

5.5 Disassembly of Layered Magnetic Micro-Modules

For Mag- μ Mods that are assembled in a layered fashion (as in Figure 11(a)), disassembly is performed using the method described in Section 4.6. A demonstration of disassembly is shown in Figure 20.

In the experiments, each species of Mag- μ Mod disassembles from another of the same species from an initially assembled state. Only MR1-MR3 are able to achieve the initially assembled layered state; MR4-MR6 are not stable in this configuration without the polyurethane shell to support their can-

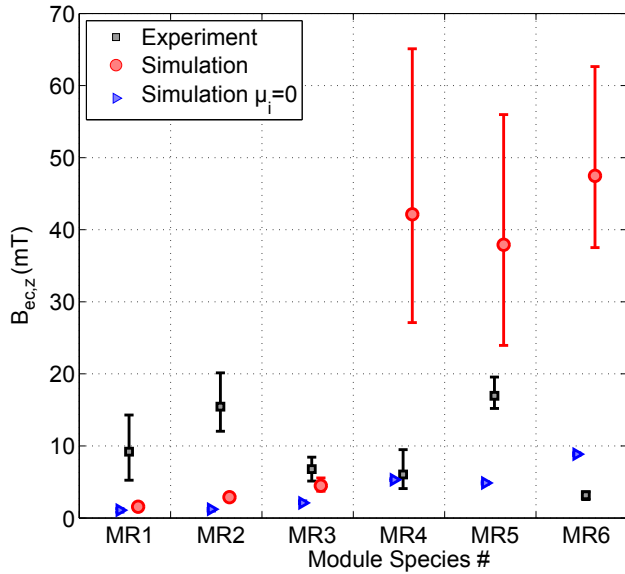


Figure 19: Experiment and simulation of the Mag- μ Mods disassembling from a planar assembly using a rotational disassembly method. In each experiment, one Mag- μ Mod is fixed on the surface, and the other is initially combined with it. Simulated data have error bars as empirically determined surface forces and friction are used in computation.

tilivered weight. Therefore, only MR1-MR3 are analyzed. The magnetic fields that begin to disassemble the Mag- μ Mods are recorded, and are compared to the estimates from the models in Section 4.6. In model computations, $F_{s,i}$ is taken as the flat-adhesion data from Figure 13, with the assumption of asperity contact, to account for the disparity in module area during the adhesion measurement, compared to the disassembly case. The results from the experiment and model are shown in Figure 21.

From these results, the predicted $B_{ec,z}$ match the experimentally determined $B_{ec,z}$ well for MR1 and MR2. The model slightly underestimates the required field for MR3. This underestimation could be due due to the small deviation in MR3 measurements in the experiment, compared to MR1 or MR2. One possibility for this result is that insufficient disassembly attempts were performed, and a very particular case was being

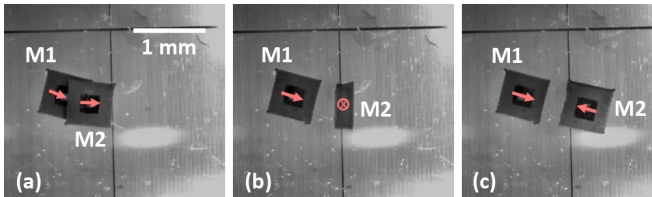


Figure 20: Frames from a movie showing two Mag- μ Mods (species MR2), M1 (anchored) and M2 (unanchored), disassembling from a layered configuration (video available in Extension 2). (a) Initial configuration. (b) M2 rotates into a vertical orientation with magnetization into the page, and rotates further in (c) until it is in a repulsive orientation with M1. Direction of magnetization is shown on each module.

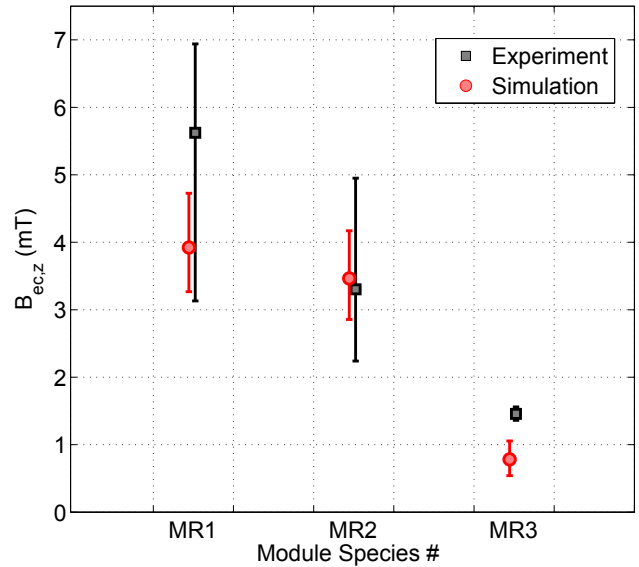


Figure 21: Experiment and simulation of the Mag- μ Mods disassembling from a layered assembly using a rotational disassembly method. In each experiment, one Mag- μ Mod is fixed on the surface, and the other is initially combined with it. Simulated data have error bars as empirically determined surface forces and friction are used in computation. Only MR4-MR6 were not capable of being assembled in a layered fashion, and are not shown.

repeated, which may not be entirely representative. For example, this disassembly method depends on the adhesion between modules, which acts as a torque. The location of this adhesive force is taken to be at the center of the overlap of the two modules (as in Figure 11(a)), however in reality, will depend on the positions of the asperities, an unknown. If in the experiment, the location of the asperities that were in contact between the two modules happened to be in the same place in all trials, then the deviation in the result can be low. However, if the modules were flipped so that different surfaces of the modules were in contact, then the location of the asperities is likely to be different, and will result in a different $B_{ec,z}$.

5.6 Capabilities

Larger, complex assemblies of many Mag- μ Mods can be formed, as shown in Figure 22, where eight Mag- μ Mods are utilized in a preliminary study. These modules create a layered structure that can be reconfigured into several morphologies, and be disassembled into their individual components.

6 Conclusions and Future Work

This paper presented the analysis of a reconfigurable robotic system at the micro-scale. This system allowed for the deterministic assembly and disassembly of several species of modules. The relevant physics was discussed and models for the assembly and disassembly tasks were developed. A method utilizing magnetics to infer adhesion, friction and weight *in-situ*

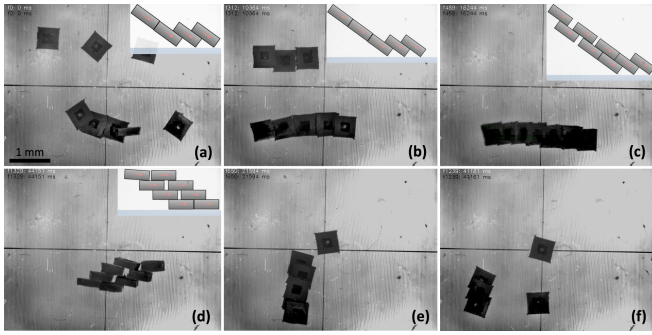


Figure 22: Frames from a movie with eight Mag- μ Mods (species MR2) assembling into a reconfigurable structure (video available in Extension 1). (a) Four Mag- μ Mods are assembled into a mobile configuration. Inset shows a schematic side-view of the assembly. (b) Two separate Mag- μ Mod assemblies are formed, one with five modules, and the other with three. Both assemblies are mobile. (c) The two assemblies combine into a larger assembly. (d) The eight-module assembly reconfigures into a different morphology, which continues to be mobile. (e) The process of disassembly begins, and one module is detached. (f) More modules are detached from the assembly.

at the micro-scale was proposed and used to infer the interactions between the modules and their environment. With further validation, this method could potentially be a useful tool for determining the properties of micro-scale objects.

The conditions required to assemble and disassemble modules were reported and compared with the proposed model. While the model accurately predicted the module behavior for two cases, one module disassembly case contained errors. In several areas, the primary suspect for differences between simulated and experimental results is fabrication inconsistencies, which could lead to variations in surface roughness, magnetization strength, and the distribution of mass. Efforts will be made in the future to improve fabrication techniques so as to create more homogeneous devices. Such improvements should not only improve the performance on individual devices, but strengthen the value of the models presented in this work as useful predictive tools.

As a mobile reconfigurable system at the micrometer scale, the Mag- μ Mod system is a step towards the creation of larger programmable reconfigurable assemblies with fine resolution. Future work will involve the creation of assemblies in 3-D; the model developed in this paper can give insight for the design of such assemblies. The stability of such assemblies must be studied and methods to deterministically create arbitrary shapes developed. These shapes can then be designed to be useful tools such as grippers, pushers, valves and pumps.

Additionally, the strength of module assemblies can be improved. As presented here, magnetic forces dominate the attraction between modules, but these forces may be relatively too weak to support the assembly for applications requiring high mechanical stresses to be applied. For such applications, stronger attachment methods need to be developed to “lock” the modules together using chemical bonds, capillary forces, or

other means.

The resolution of the Mag- μ Mod system could also be increased by scaling the modules smaller, although several new challenges may present themselves. The relative magnitude of surface forces will increase and magnetic attractive forces will reduce, so the inter-module attractive forces would need to be modified to account for this. Additionally, the micro-scale molding technique used in this paper may not be appropriate for modules smaller than $100\ \mu\text{m}$, so other fabrication techniques may need to be used.

Funding

This work is supported by the National Science Foundation CAREER award program [NSF IIS-0448042], and the NSF Graduate Research Fellowship.

Conflict of interest statement

None declared.

Acknowledgement

The authors would like to thank the NanoRobotics Laboratory members for their support and suggestions, Magnequench, Inc. for supplying magnetic powder and Andrew Gamble and the Carnegie Mellon DSSC for use of the vibrating sample magnetometer

References

- J. J. Abbott, K. E. Peyer, M. C. Lagomarsino, L. Zhang, L. Dong, I. K. Kaliakatsos, and B. J. Nelson. How Should Microrobots Swim? *International Journal of Robotics Research*, 28(11-12):1434–1447, July 2009.
- B. Behkam and M. Sitti. Bacterial flagella-based propulsion and on/off motion control of microscale objects. *Applied Physics Letters*, 90:023902, 2007.
- K.-F. Bohringer. Programmable Force Fields for Distributed Manipulation, with Applications to MEMS Actuator Arrays and Vibratory Parts Feeders. *The International Journal of Robotics Research*, 18(2):168–200, Feb. 1999.
- D. K. Cheng. *Field and Wave Electromagnetics, 2nd Edition*. Addison-Wesley Publishing Company, Inc., 1992.
- B. Donald, C. Levey, C. McGray, I. Paprotny, and D. Rus. An untethered, electrostatic, globally controllable MEMS micro-robot. *Journal of Microelectromechanical Systems*, 15:1–15, 2006.
- B. Donald, C. Levey, and I. Paprotny. Planar microassembly by parallel actuation of MEMS microrobots. *Journal of Microelectromechanical Systems*, 17:789–808, 2008.

- O. Ergeneman, G. Dogangil, M. P. Kummer, J. J. Abbott, M. K. Nazeeruddin, and B. J. Nelson. A magnetically controlled wireless optical oxygen sensor for intraocular measurements. *IEEE Sensors Journal*, 8:2022–2024, 2008.
- S. Floyd, C. Pawashe, and M. Sitti. Two-dimensional contact and non-contact micro-manipulation in liquid using an untethered mobile magnetic micro-robot. *IEEE Transactions on Robotics*, 25:1332–1342, 2009.
- S. C. Goldstein, J. D. Campbell, and T. C. Mowry. Programmable matter. *Computer*, 38:99–101, 2005.
- M. Imbaby, K. Jiang, and I. Chang. Net shape fabrication of stainless-steel micro machine components from metallic powder. *Journal of Micromechanics and Microengineering*, 18:115018, 2008.
- J. Israelachvili. *Intermolecular and Surface Forces*. Academic Press, 1992.
- M. Kalontarov, M. T. Tolley, H. Lipson, and D. Erickson. Hydrodynamically driven docking of blocks for 3D fluidic assembly. *Microfluidics and Nanofluidics*, 9(2-3):551–558, 2010.
- S. Martel, O. Felfoul, J.-B. Mathieu, A. Chanu, S. Tamaz, M. Mohammadi, M. Mankiewicz, and N. Tabatabaei. MRI-based Medical Nanorobotic Platform for the Control of Magnetic Nanoparticles and Flagellated Bacteria for Target Interventions in Human Capillaries. *International journal of robotics research*, 28:1169–1182, 2009.
- M. Mastrangeli, S. Abbasi, C. Varel, C. Van Hoof, J.-P. Celis, and K. F. Bohringer. Self-assembly from milli- to nanoscales: methods and applications. *Journal of Micromechanics and Microengineering*, 19(8):083001, July 2009.
- C. Pawashe, S. Floyd, and M. Sitti. Multiple magnetic micro-robot control using electrostatic clamping. *Applied Physics Letters*, 94:164108, 2009a.
- C. Pawashe, S. Floyd, and M. Sitti. Assembly and Disassembly of Magnetic Mobile Micro-Robots towards 2-D Reconfigurable Micro-Systems. *Proceedings of the International Symposium on Robotics Research*, 70:731–747, 2009b.
- C. Pawashe, S. Floyd, and M. Sitti. Modeling and Experimental Characterization of an Untethered Magnetic Micro-Robot. *International Journal of Robotics Research*, 28(8):1077–1094, 2009c.
- T. Sawetzki, S. Rahmouni, C. Bechinger, and D. W. M. Marr. In situ assembly of linked geometrically coupled microdevices. *Proceedings of the National Academy of Sciences*, 105(51):20141–5, Dec. 2008.
- W.-M. Shen, H. Chiu, M. Rubenstein, and B. Salemi. Rolling and climbing by the multifunctional superbot reconfigurable robotic system. In *Proceedings of the Space Technology International Forum*, pages 839–848, Albuquerque, New Mexico, 2008.
- M. Sitti. Microscale and nanoscale robotics systems [grand challenges of robotics]. *Robotics Automation Magazine, IEEE*, 14(1):53–60, March 2007.
- M. Sitti. Voyage of the microrobots. *Nature*, 458:1121–1122, April 2009.
- O. Sul, M. Falvo, R. Taylor, S. Washburn, and R. Superfine. Thermally actuated untethered impact-driven locomotive microdevices. *Applied Physics Letters*, 89:203512, 2006.
- M. T. Tolley, M. Krishnan, D. Erickson, and H. Lipson. Dynamically programmable fluidic assembly. *Applied Physics Letters*, 93(25):254105, 2008.
- K. Vollmers, D. Frutiger, B. Kratochvil, and B. Nelson. Wireless resonant magnetic microactuator for untethered mobile microrobots. *Applied Physics Letters*, 92:144103, 2008.
- M. Yim, W.-M. Shen, B. Salemi, D. Rus, M. Moll, H. Lipson, E. Klavins, and G. S. Chirikjian. Modular self-reconfigurable robot systems. *IEEE Robotics and Automation Magazine*, 14:43–52, 2007.
- E. Yoshida, S. Kokaji, S. Murata, K. Tomita, and H. Kurokawa. Micro self-reconfigurable robot using shape memory alloy. *Journal of Robotics and Mechatronics*, 13:212–219, 2001.

Appendix: Index to Multimedia Extensions

The multimedia extensions to this article are at <http://www.ijrr.org>.

Table of Multimedia Extensions

Extension	Type	Description
1	Video	Mag- μ Mod demonstration video, including assembly, reconfiguring and disassembly tasks, corresponding to Figs. 3 and 22.
2	Video	Video of assembly and planar and layered disassembly experiments, corresponding to Figs. 15, 18 and 20, respectively.
3	Data	Experimental data for adhesion, friction, assembly and disassembly experiments. Includes measured field strength and field gradient.